Crystallinity and Oxygen Transport Properties of PET Bottle Walls

R. Y. F. Liu, Y. S. Hu, D. A. Schiraldi, A. Hiltner, E. Baer

Department of Macromolecular Science and Center for Applied Polymer Research, Case Western Reserve University, Cleveland, Ohio 44106-7202 USA

Received 26 March 2004; accepted 29 April 2004
DOI 10.1002/app.20905
Published online in Wiley InterScience (www.interscience.wiley.com).

ABSTRACT: Oxygen transport was coupled with other methods to study the relationship of gas barrier to solid state structure in the PET blown bottle wall. Commercial 2-L carbonated soft drink bottles blown under different process conditions were studied. Crystallinity determinations from heat of melting, density, glycol *trans* fraction, and oxygen solubility were compared. The reasons for lack of correlation between conventional crystallinity methods based on heat of melting and density were elucidated, and neither was found to be reliable. An alternative approach to determining crystallinity based on oxygen solubility gave reliable results and revealed fundamental characteristics of the amorphous phase, such as amorphous phase density and amorphous phase oxygen solubility. Dedensification of the amorphous phase was responsible for higher oxygen permeability of bottle walls processed under conditions of higher thermal exposure (temperature/time) despite the parallel increase in volume fraction of impermeable crystals. The strong dependence of dedensification on process temperature was explained in terms of the temperature–volume relationship of the amorphous phase. A low process temperature minimized amorphous phase dedensification and delivered a bottle wall with the best oxygen barrier. © 2004 Wiley Periodicals, Inc. J Appl Polym Sci 94: 671–677, 2004

Key words: polyesters; gas permeation; barrier; blown bottle; orientation

INTRODUCTION

Poly(ethylene terephthalate) (PET) is widely used in bottles for food and beverage packaging. High orientation and strain-induced crystallization imparted by the stretch–blow molding process give the bottle improved oxygen barrier over unoriented, amorphous PET.[1] Efforts to quantify biaxial orientation reveal complex orientation patterns in the bottle and strong orientation gradients through the bottle wall.[2] The latter arise from the nonuniform temperature distribution through the thick bottle perform and can affect mechanical, barrier, and optical properties of the bottle wall.[3]

Because of orientation gradients inherent to the bottle wall, efforts to quantify interrelationships among process variables, such as temperature and rate, the degree of molecular orientation, and the resulting physical properties have focused on characterization of oriented film or sheet. Although a large literature addresses orientation of PET, studies most relevant to blown bottles are those that concern development of strain-induced crystallization,[4,5] and those that focus on biaxial orientation.[6,7] These studies can be the basis for predicting mechanical and optical properties of blown bottles from film data.[8] However, basic understanding of the relationship between solid state structure and gas permeability, which could lead to quantitative models for predicting gas permeability of PET bottles, is not available.

Strain-induced crystallization and amorphous phase orientation imparted by the blowing process provide the reduced gas permeability of bottles compared to amorphous PET. Crystallization reduces the volume fraction of permeable amorphous phase available for gas transport. However, reliable determination of volume fraction crystallinity in bottle wall remains elusive, as standard methods based on heat of melting and density are not in good agreement.[9–12] Density of the permeable amorphous phase reflects the amount of excess hole free volume available for sorption and diffusion of gas molecules. Orientation of PET without crystallization increases the amorphous density, thereby reducing the permeability.[13,14] However, it is well known that the amorphous phase of PET readily dedensifies during crystallization,[15] thereby increasing the permeability of the amorphous phase and mitigating to some extent the other effects of orientation and crystallization.[10–12] Considering that the bottle experiences both crystallization and orientation during the blowing process, it is not surprising that the rela-

Correspondence to: A. Hiltner (pah6@cwru.edu).

tionship between gas transport and solid state structure is a complex one.

In addition to being an important performance property, oxygen permeability becomes a powerful structural probe when separated into its thermodynamic and kinetic components of gas solubility and gas diffusivity. At low pressure, gas permeability is viewed as a jumping process whereby a penetrant molecule spends most of the time in free-volume holes and occasionally jumps into a neighboring hole by formation of a connecting channel. Gas solubility measures the amount of free volume, whereas diffusivity measures the frequency of channel formation. The utility of gas transport as a probe of the amorphous phase is amply demonstrated in studies of orientation[13,14] and crystallization of PET[10–12] and other aromatic polyesters.[16,17]

In the present study, we use oxygen transport coupled with other methods to understand gas barrier of the PET blown bottle wall in terms of the solid state structure. Commercial 2-L carbonated soft drink bottles blown at different temperatures are studied. The amorphous phase is characterized in terms of density, free volume, and oxygen solubility. Comparisons among crystallinity determinations from heat of melting, density, glycol *trans* fraction, and oxygen solubility are made. Correlations between oxygen transport properties and the structural parameters induced by blowing conditions are presented.

METHODS

Two-liter carbonated soft drink bottles were supplied by KoSa (Spartanburg, SC). The PET bottles were blown from preforms using a commercial blow molding machine (Sidel). The side wall temperatures were nominally 90°C (cold-blown bottle) or 105°C (hot-blown bottle). The blowing cycle time was 3 s. Another bottle was held for an additional 1.5 s after being blown at 105°C (heat-set bottle). A bottle made from a blend of PET and poly(ethylene isophthalate) (PEI) with 90/10 (wt/wt) composition was blown at 98°C (blend-10I bottle). The bottle-wall draw ratio of 2.5 $\times$ 4.0 (length $\times$ hoop) was typical of commercial bottle production. The wall section was cut from the bottle for subsequent characterization.

An amorphous PET film was obtained by compression molding followed by quenching from the melt. The film was cold-drawn at 59°C under constrained uniaxial conditions to a target draw ratio of 4 using a strain rate of 20% min^{-1} as described previously.[13]

Differential scanning calorimetry (DSC) was carried out in a Perkin–Elmer DSC7 calibrated with indium and tin standards. All tests were performed in a nitrogen atmosphere. The heating rate was 10°C min^{-1} in the range of 30 to 275°C.

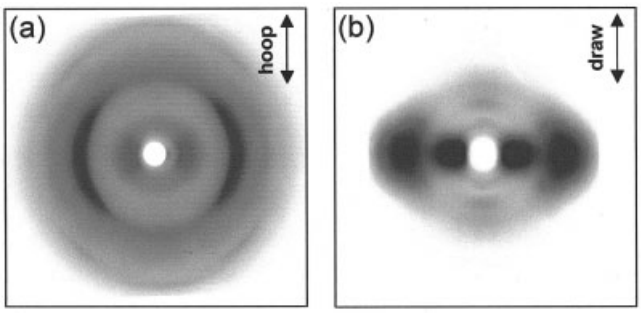

Figure 1 Wide angle X-ray diffraction patterns: (a) cold-blown bottle wall and (b) cold-drawn PET film.

Two-dimensional wide angle X-ray diffraction (WAXD) patterns were obtained using a Statton camera and Ni-filtered Cu Kα radiation calibrated with calcium fluoride.

A density gradient column was constructed from a solution of calcium nitrate and water in accordance with ASTM D Standard 1505 Method B. The column was calibrated with glass floats of known density. The density accuracy for bottle walls was $\pm$ 0.001 g cm^{-3}.

Fourier transform infrared spectra were analyzed for conformational composition as described previously.[13] Spectra were collected at ambient temperature with a Nicolet 870 Fourier transform infrared spectrometer with an MTEC model 200 photoacoustic cell. The fractions of *gauche*- and *trans*-glycol conformations were obtained from the relative intensity of peaks at 1456 and 1476 cm^{-1}.

Oxygen flux $J(t)$ at 0% relative humidity, 1 atm pressure, and 23°C was measured with a MOCON OX-TRAN 2/20. Specimens were carefully conditioned as described previously.[10] Diffusivity D and permeability P were obtained by fitting the nonsteady state flux versus time curve to the solution to Fick's second law with appropriate boundary conditions.[10] The thickness l of each specimen was determined from the measured density after the barrier measurement was completed.

RESULTS AND DISCUSSION

Crystallinity of bottle walls

The X-ray diffraction pattern of the cold-blown bottle wall is shown in Figure 1(a). The fiber-like pattern revealed strain-induced crystallization and unbalanced orientation of the bottle wall with higher extension in the hoop direction than in the length direction. The other bottle walls gave virtually the same pattern. By drawing constrained PET films using a relatively low strain rate, it was possible to draw PET below T_g without causing cavitation. The X-ray pattern in Figure 1(b) shows that drawing at 59°C (cold-drawn PET) oriented the chains without inducing crystallization.

TABLE I
Properties of Blow-Molded Bottle Walls

Property	Glassy PET	Cold-Drawn Film	Cold-Blown Bottle	Hot-Blown Bottle	Heat-Set Bottle	Blend-10I Bottle
ΔH_{cc} (J g^{-1})	34	3	3	2	0	2
ΔH_m (J g^{-1})	35	47	44	46	47	41
$\phi_{c,m}$	0.01	0.35	0.33	0.35	0.38	0.31
$\phi_{c,\rho}$	0.00	0.12	0.19	0.21	0.23	0.23
ϕ_c	0.00	0.00	0.22	0.29	0.34	0.27
f_t	0.08	0.27	0.33	0.36	0.44	0.40
ρ (g cm^{-3})	1.337	1.354	1.364	1.366	1.369	1.369
ρ_a (g cm^{-3})	1.337	1.354	1.332	1.321	1.315	1.329
P	0.424	0.201	0.171	0.219	0.236	0.167
D	5.0	4.0	2.5	2.8	3.0	2.4
S	0.098	0.058	0.080	0.089	0.092	0.080
S_a	0.098	0.058	0.103	0.125	0.139	0.110
FFV	0.036	0.022	0.040	0.048	0.053	0.042

P, permeability cc(STP) cm m^{-2} day^{-1} atm^{-1};
D, diffusivity 10^{-13} m^2 s^{-1};
S, solubility cc(STP) cm^{-3} atm^{-1}.

Molecular simulations also suggest that PET chains can be in an oriented state without crystalline registration.[18]

The infrared spectra were analyzed for the fraction of *trans* conformations f_t using the method previously developed for PET and other aromatic polyesters.[13] Orientation increased the *trans* fraction from 0.08 for glassy PET to 0.27 for cold-drawn PET film. Crystallization increased the *trans* fraction further to 0.44 for heat-set bottle (Table I). Because the contributions of crystallization and orientation to the increase in *trans* fraction could not be separated, this approach was not considered further as a method for determining crystallinity of bottle wall.

The DSC thermograms of all the bottle walls and the cold-drawn film were similar despite the significant differences in process history (Figure 2). All the thermograms except that of the heat-set bottle included a small crystallization exotherm immediately following the glass transition. The heat of cold crystallization ΔH_{cc} was subtracted from the melting enthalpy ΔH_m to obtain the volume fraction crystallinity $\phi_{c,m}$ as

$$\phi_{c,m} = \frac{\rho}{\rho_c}\frac{\Delta H}{\Delta H^o} \quad (1)$$

where ρ is the measured density, ρ_c is the density of the PET crystal taken as 1.476 g cm^{-3}, $\Delta H = \Delta H_m - \Delta H_{cc}$, and ΔH^o is the heat of fusion of the PET crystal taken as 125 J g^{-1}.[19] All the PET bottle walls and the cold-drawn PET film had about the same volume fraction crystallinity from ΔH, 0.33–0.38 (Table I). The volume fraction crystallinity of the blend bottle was only slightly lower, 0.31.

Volume fraction crystallinity was also calculated from density $\phi_{c,\rho}$ according to

$$\phi_{c,\rho} = \frac{\rho - \rho_a}{\rho_c - \rho_a} \quad (2)$$

where ρ_a and ρ_c are taken as 1.337 and 1.476 g cm^{-3} for amorphous and crystalline phases, respectively. Crystallinity from density was considerably lower than crystallinity from ΔH. The volume crystallinity calculated from density increased slightly with the bottle process temperature from 0.19 for cold-blown bottle to 0.23 for heat-set bottle (Table I). Density crystallinity also differentiated the bottles from cold-drawn film, which had crystallinity from density of 0.12.

There are compelling reasons to mistrust both methods of crystallinity determination. During heating, oriented amorphous chains transform into three-dimensional crystals, thereby increasing the heat of melting.[9,20,21] On the other hand, numerous studies reveal that the amorphous phase density of PET and other aromatic polyesters cannot be assumed to be constant.[10–12,15,16] Orientation increases amorphous phase density due to transformation of some *gauche* conformers to *trans* conformers. In contrast, crystallization decreases amorphous phase density due to constraint on amorphous chain segments attached to chain segments in crystals. Gas transport has been a particularly powerful technique for probing the amorphous phase of variable density.

Oxygen transport

Gas transport behavior of crystalline polyesters is often interpreted in terms of a two-phase structural model consisting of an impermeable crystalline phase dispersed in a permeable amorphous matrix. Thus, both sorption and diffusion are seen as taking place in

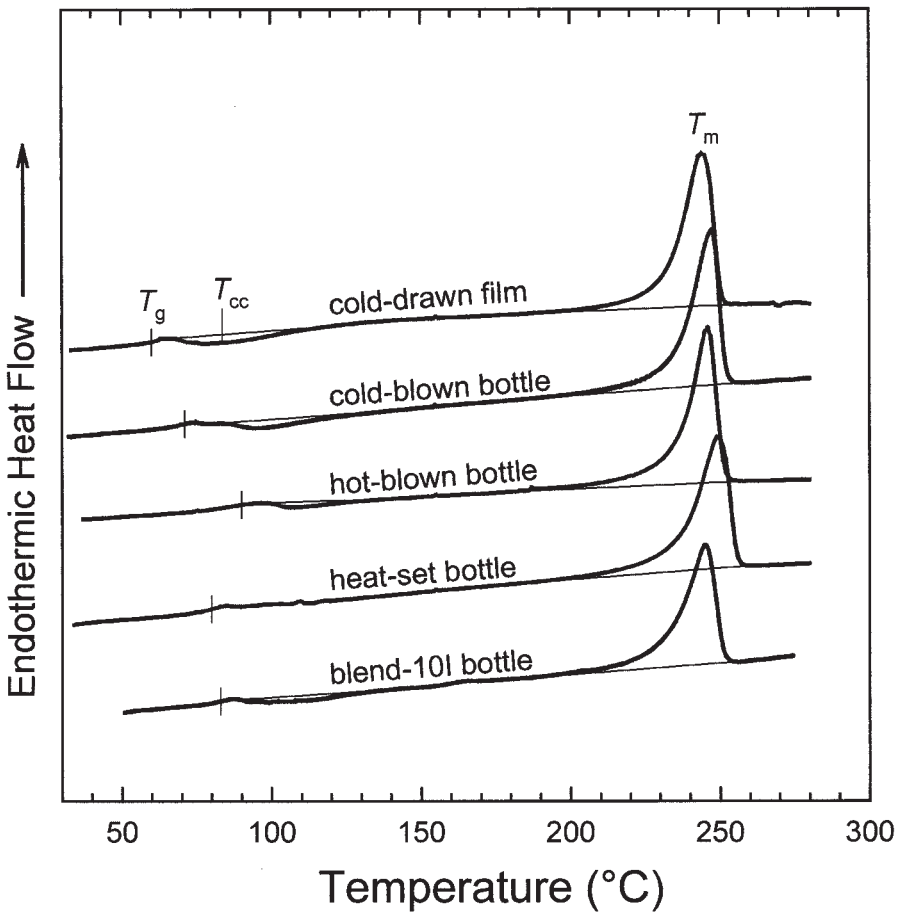

Figure 2 DSC thermograms obtained at a heating rate of 10°C min^{-1}.

the amorphous phase. Solubility in the amorphous phase, S_a, is obtained by normalizing measured bulk solubility S to the volume fraction of amorphous phase

$$S_a = \frac{S}{1 - \phi_c} \tag{3}$$

where ϕ_c is the volume crystallinity. However, as a consequence of the variable amorphous phase density, a unique value of S_a does not describe the amorphous phase of PET.

A linear relationship between amorphous oxygen solubility S_a and amorphous specific volume $\nu_a(=\rho_a^{-1})$ has been observed for glassy copolymers of PET,[22,23] for cold-drawn PET, PEN, and a PET copolymer,[13,14] and for the amorphous phase of crystallized PET[10,11] and PEN.[16] The linear relationship appears to be a common characteristic of polyesters of ethylene glycol and aromatic diacids. The general correlation between S_a and ν_a is expressed as

$$S_a = \beta(\nu_a - \nu_o) \tag{4}$$

where ν_o is the specific volume at zero solubility. According to free volume concepts that view sorption as the process of filling holes of static free volume, the quantity $(\nu_a - \nu_o)$ identifies the hole free volume ν_f available to oxygen.[13,14,22] Furthermore, fractional free volume (FFV) can be calculated as $FFV = \nu_f/\nu_a$. Orientation of the glassy state decreases the hole free volume, whereas crystallization often has the effect of increasing the hole free volume of the amorphous phase. The extrapolated quantity ν_o is not necessarily the same for all polyesters and reflects a characteristic of the particular chemical structure. However, the slope β is about 3.6 cc(STP) g cm^{-6} atm^{-1} at 23°C for all the aromatic polyesters studied. This slope reflects the density of sorbed oxygen, and constant β indicates fundamental similarity in the characteristics of the accessible free volume in the amorphous phase.[14,22]

The impact of amorphous phase dedensification is illustrated by considering oxygen solubility S of bottle walls. All possessed some amount of strain-induced crystallization. Intuitively, oxygen solubility should decrease with increasing density due to reduction in volume fraction amorphous phase. However, the op-

posite was observed: the higher the bottle wall density, the higher the oxygen solubility to the extent that heat-set bottle wall had oxygen solubility almost equal to that of glassy PET (Table I). This unusual result reflected a dramatic increase in oxygen solubility in the amorphous phase due to a decrease in amorphous phase density.

Following the previous approach used with PET,[10,11] analysis was carried out with a two-phase model with constant crystalline phase density ρ_c taken as 1.476 g cm^{-3}, which is considered intrinsic for the defective crystalline phase of PET,[15] and a variable amorphous phase density $\rho_a(\rho)$. For a given bulk density ρ, the value of ρ_a is given as

$$\rho_a = \frac{\rho - \rho_c\phi_c}{1 - \phi_c} \tag{5}$$

Equations (3), (4), and (5) contain three unknowns: ρ_a, ϕ_c, and S_a. They can be solved simultaneously with known constants β (3.6 cc(STP) g cm^{-6} atm^{-1}), ν_o (0.722 cm^3 g^{-1}), and ρ_c (1.476 g cm^{-3}) and experimentally determined S and ρ. The results for ρ_a, ϕ_c, and S_a are summarized in Table I.

Orientation by cold-drawing densified PET without crystallization. The increase in density from 1.337 to 1.354 g cm^{-1} reduced S from 0.098 to 0.058 cc(STP) cm^{-3} in accordance with eq. (4). However, the bottle-blowing process both oriented and crystallized PET. Results for ρ_a in Table I indicated no instances in which the bottle process increased the amorphous phase density. Instead, all the bottle walls exhibited some level of amorphous phase dedensification. Increasing thermal exposure (temperature/time) of the bottle wall enhanced dedensification of the amorphous phase and increased amorphous phase oxygen solubility. Thus, for cold-blown, hot-blown, and heat-set bottle walls, amorphous phase density decreased from a typical value for glassy PET of 1.337 to 1.332, 1.321 and 1.315 g cm^{-3}, and amorphous phase oxygen solubility increased accordingly from 0.098 to 0.103, 0.125 and 0.139 cc(STP) cm^{-3}. The corresponding increase in amorphous phase fractional free volume *FFV* is included in Table I.

The resulting volume fraction crystallinity ϕ_c from gas solubility was also strongly dependent on processing history, increasing as 0.22, 0.29, and 0.34 for cold-blown, hot-blown, and heat-set bottle walls, respectively. Cold-blown bottle experienced the least dedensification, thus crystallinity from the two-phase density model using a typical density value for amorphous PET gave a good result ($\phi_{c,\rho}$ of 0.19 compared to ϕ_c of 0.22). Because of the low process temperature, this bottle wall also underwent the most extensive thermal reorganization during the heating thermogram and therefore crystallinity from heat of melting was unreliable ($\phi_{c,m}$ of 0.33 compared to ϕ_c of 0.22). The reverse was true for heat-set bottle wall. Crystallinity from density was unreliable due to considerable dedensification of the amorphous phase ($\phi_{c,\rho}$ of 0.23 compared to ϕ_c of 0.34). On the other hand, this bottle wall underwent the least amount of thermal reorganization during the heating thermogram, and therefore heat of melting gave a good result ($\phi_{c,m}$ of 0.38 compared to ϕ_c of 0.34). Neither density nor heat of melting gave a good result for hot-blown bottle, which had intermediate ϕ_c of 0.29, or for blend-10I bottle, which had ϕ_c of 0.27. Although conventional methods of determining crystallinity from density and heat of melting may give correct results in specific cases, neither should be considered as a reliable method for determining crystallinity of PET blown bottle walls.

The effect of dedensification on S_a was large enough that bulk solubility S increased with increasing thermal exposure (temperature/time) despite the parallel decrease in volume fraction of permeable amorphous phase ($1 - \phi_c$) (Table I). The bulk diffusivity D also increased (Table I). As a result of the combined effects of dedensification on S and D, oxygen permeability P systematically increased as 0.171, 0.219, and 0.236 cc(STP) cm m^{-2} day^{-1} atm^{-1} for cold-blown bottle, hot-blown bottle, and heat-set bottle, respectively. It should be noted, however, that the heat-set bottle wall also had the greatest thermal stability. Introduction of isophthalate into PET by either copolymerization or blending decreases oxygen permeability due to decreases in both D and S.[22,24] The effect is seen with the lower permeability of the blend bottle wall.

The temperature–volume relationship

An increase in specific volume of the amorphous phase with crystallization is attributed to constraint on relaxation of amorphous chain segments imposed by their attachment to chain segments in crystals. The effect of constraint on amorphous PET chains can be discussed in terms of the temperature–volume relationship in Figure 3. During cooling, unconstrained amorphous chains contract along the equilibrium liquid line (bold solid line in Fig. 3) to the normal glass transition temperature T_g, then along the unconstrained nonequilibrium glassy line (bold dashed line in Fig. 3) to ambient temperature. Orientation by cold-drawing decreases the hole free volume bringing the nonequilibrium glass closer to the equilibrium line.[13,14] However, in the bottle wall, amorphous chain segments are attached to chain segments in crystals. As the bottle wall is cooled from the process temperature, amorphous chain segments lack mobility to relax along the liquid line; instead, they are immobilized much as they would be in the glassy state. During cooling from the process temperature, contraction along a line parallel to the normal glassy line increases

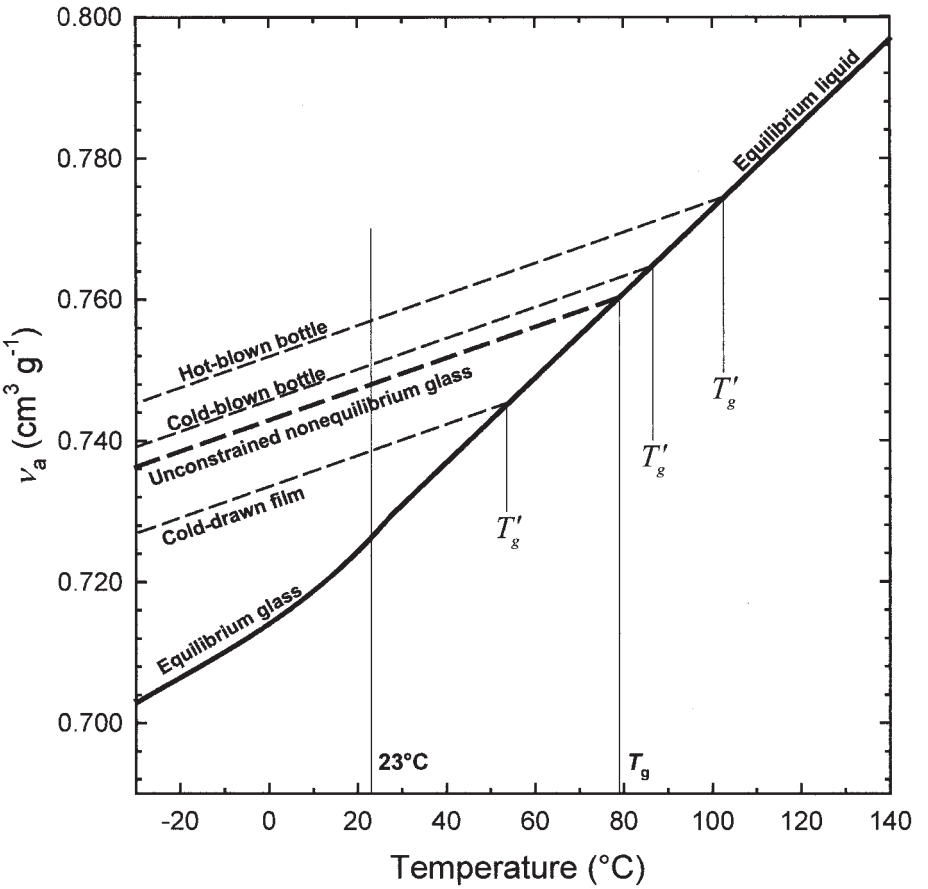

Figure 3 Temperature versus amorphous specific volume relationship for PET.

the hole free volume bringing the nonequilibrium glass further from the equilibrium line. The additional hole free volume resulting from constraint $\Delta\nu_f$ is the difference between the dedensified amorphous specific volume and the specific volume of the unconstrained glass ν_g.

It follows from the concept of the amorphous phase as presented in Figure 3 that the glass transition temperature should decrease with densification of the glass and should increase with dedensification. Indeed, this is observed in the DSC thermograms (Fig. 2). Cold-drawn PET has the lowest T_g, lower than the normal T_g of glassy PET. The T_g inflection of cold-blown bottle is somewhat higher and the T_g of hot drawn bottle is even higher.

Furthermore, the effective glass transition temperature T_g', which should be equal to the nominal process temperature T_p, can be derived from the temperature–volume relationship and ν_a according to

$$T_g' = T_g + \frac{\nu_a - \nu_g}{\Delta e} \tag{6}$$

where Δe is the difference between the specific thermal expansivities of equilibrium liquid and glass, taken as 3.6×10^{-4} cm^3 g^{-1} K^{-1}, T_g is the normal glass transition temperature of PET taken as 79°C, and ν_g is the specific volume of glassy PET taken as 0.748 cm^3 g^{-1}. Calculated values of T_g' from eq. (6) were 53, 87, and 104°C for cold-drawn film, cold-drawn bottle and hot-drawn bottle, respectively, in excellent agreement with the nominal process temperatures of 59, 90, and 105°C, respectively. Assuming the same properties for the blend, the agreement was almost as good, with T_g' from eq. (6) of 91°C compared to the nominal process temperature of 98°C. The agreement emphasizes the key role of blow temperature in determining the amorphous phase properties of the bottle wall.

CONCLUSION

This study probes the solid state structure of PET bottle wall and its relationship to oxygen transport properties using commercially blown bottles. Various methods for determining the amount of strain-induced crystallinity are compared. The reasons for lack of correlation between conventional methods based on heat of melting and density are elucidated, and neither is found to be reliable. Crystallinity from heat of melting does not accommodate transformation of oriented

chains into crystallites as the heating thermogram is recorded and tends to overestimate crystallinity. Density crystallinity based on constant crystalline and amorphous phase densities does not accommodate dedensification of the amorphous phase of crystallized PET and therefore tends to underestimate crystallinity. Measurement of oxygen solubility is shown to provide a reliable crystallinity determination and also reveals fundamental characteristics of the amorphous phase, such as amorphous phase density and amorphous phase oxygen solubility. Dedensification of the amorphous phase is due to constraint on amorphous chains attached to chain segments in crystals. The strong dependence of dedensification on process temperature is explained in terms of the temperature–volume relationship of the amorphous phase. Amorphous phase dedensification is responsible for increased oxygen permeability of bottle walls processed under conditions of higher thermal exposure (temperature/time) despite the parallel increase in volume fraction of impermeable crystals. A low process temperature minimizes amorphous phase dedensification and delivers a bottle wall with the best oxygen barrier.

This research was generously supported by KoSa. Support from Modern Controls, Inc. for development of a facility for gas-transport studies at Case Western Reserve University is gratefully acknowledged.

References

1. Swaroop, N.; Gordon, G. A. Polym Eng Sci 1980, 20, 78.
2. Everall, N.; MacKerron, D.; Winter, D. Polymer 2002, 43, 4217.
3. Venkateswaran, G.; Cameron, M. R.; Jabarin, S. A. Adv Polym Tech 1998, 17, 237.
4. Jabarin, S. A. Polym Eng Sci 1992, 32, 1341.
5. Slee, J. A.; Orchard, G. A. J.; Bower, D. I.; Ward, I. M. J Polym Sci B: Polym Phys 1989, 27, 71.
6. Orchard, G. A. J.; Spiby, P.; Ward, I. M. J Polym Sci B: Polym Phys 1990, 28, 603.
7. Chandran, P.; Jabarin, S. Adv Polym Tech 1993, 12, 153.
8. Venkateswaran, G.; Cameron, M. R.; Jabarin, S. A. Adv Polym Tech 1998, 17, 217.
9. Bashir, Z.; Al-Aloush, I.; Al-Raqibah, I.; Ibrahim, M. Polym Eng Sci 2000, 40, 2442.
10. Sekelik, D. J.; Stepanov, E. V.; Nazarenko, S.; Schiraldi, D.; Hiltner, A.; Baer, E. J Polym Sci B: Polym Phys 1999, 37, 847.
11. Polyakova, A.; Stepanov, E. V.; Sekelik, D.; Schiraldi, D. A.; Hiltner, A.; Baer, E. J Polym Sci B: Polym Phys 2001, 39, 1911.
12. Lin, J.; Shenogin, S.; Nazarenko, S. Polymer 2002, 43, 4733.
13. Liu, R. Y. F.; Schiraldi, D. A.; Hiltner, A.; Baer, E. J Polym Sci B: Polym Phys 2002, 40, 862.
14. Liu, R. Y. F.; Hiltner, A.; Baer, E. J Polym Sci B: Polym Phys 2004, 42, 493.
15. Bornschlegl, E.; Bonart, R. Colloid Polym Sci 1980, 258, 319.
16. Hu, Y. S.; Liu, R. Y. F.; Zhang, L. Q.; Rogunova, M.; Schiraldi, D. A.; Nazarenko, S.; Hiltner, A.; Baer, E. Macromolecules 2002, 35, 7326.
17. Hu, Y. S.; Liu, R. Y. F.; Rogunova, M.; Schiraldi, D. A.; Nazarenko, S.; Hiltner, A.; Baer, E. J Polym Sci B: Polym Phys 2002, 40, 2489.
18. Tonelli, A. E. Polymer 2002, 43, 637.
19. Wunderlich, B. Macromolecular Physics; Academic Press: New York, 1973; vol. 1, p. 389.
20. Parravicini, L.; Leone, B.; Auriemma, F.; Guerra, G.; Petraccone, V.; Didino, G.; Bianchi, R.; Vosa, R. J Appl Polym Sci 1994, 52, 875.
21. Busico, V.; Corradini, P.; Riva, F.; Seves, A.; Vicini, L. Makromol Chem Rapid Commun 1980, 1, 423.
22. Polyakova, A.; Liu, R. Y. F.; Schiraldi, D. A.; Hiltner, A.; Baer E. J Polym Sci B: Polym Phys 2001, 39, 1889.
23. Polyakova, A.; Connor, D. M.; Collard, D. M.; Schiraldi, D. A.; Hiltner, A.; Baer, E. J Polym Sci B: Polym Phys 2001, 39, 1900.
24. Liu, R. Y. F.; Hu, Y. S.; Schiraldi, D. A.; Hiltner, A.; Baer, E. Unpublished results.